Smart Structures and Systems, *Vol. 34, No. 4 (2024) 215-227*
https://doi.org/10.12989/sss.2024.34.4.215

Shaking table tests on vibration reduction of multi-degree-freedom structures using SMA spring-based TVA

Kunjie Rong [1a], Zhengquan Cheng [1], Mengyao Zhou*[1,2], Weiyuan Huang [2b], Ruisheng Ma [3c] and Na Li [4]

[1] *School of Civil Engineering, Shandong University, Jinan, Shandong Province, 250061, China*
[2] *Department of Disaster Mitigation for Structures, Tongji University, Shanghai, 200092, China*
[3] *Key Laboratory of Urban Security and Disaster Engineering of Ministry of Education, Beijing University of Technology, Beijing, 100124, China*
[4] *College of Civil Engineering, Qilu Institute of Technology, Jinan, Shandong Province, 250200, China*

(*Received March 29, 2024, Revised October 25, 2024, Accepted November 6, 2024*)

Abstract. This study utilizes the superelasticity property of shape memory alloy (SMA) to form a shape memory alloy spring-based tuned vibration absorber (SMA-TVA) for mitigating vibrations in multi-degree-of-freedom (MDOF) structures. Nitinol SMA is chosen for the fabrication of SMA specimens, and cyclic displacement loading tests are performed on both SMA wire and spring. Shaking table tests are then designed and executed on a three-story steel shear frame under tuned vibration absorber (TVA) and SMA-TVA control, respectively. Four seismic waves are selected to compare the performance of two dampers, with a specific focus on the time-frequency energy evolution of the MDOF structure under different excitations. Furthermore, the robustness of SMA-TVA is validated across varying excitation amplitudes and frequency ratios. Results reveal that SMA-TVA effectively attenuates vibrations beyond its tuning frequency, dissipating energy associated with multiple modes. It outperforms TVA with a significant 109.3% and 85.2% improvement in RMS displacement and acceleration reduction, respectively, with strokes reduced by up to 42.5% under earthquakes. Certain earthquakes exhibit a prolonged period of high energy input, facilitating more efficient and stable attenuation of vibrations for SMA-TVA. The average change in the vibration reduction ratio remains below 13.7% within the considered varying frequency ratios, indicating that SMA-TVA exhibits robustness against tuning frequency deviation.

Keywords: passive control; shaking table test; shape memory alloy spring; tuned vibration absorber; vibration reduction

1. Introduction

Advanced durable construction technologies have facilitated the integration of complex building structures like high-rise buildings and large cantilever structures into contemporary urban infrastructures. To decrease the unexpected vibrations of the engineering structures under dynamic loads like earthquakes and winds, vibration mitigation methods using feasible control equipment have been developed (Gur *et al*. 2014, Mohsenian *et al*. 2021). Among these methods, tuned mass damper (TMD) is commonly adopted due to its simple construction and energy input exemption. The fundamental requirement for a TMD is aligning its eigenfrequency with that of the primary structure. However, a challenge may arise if a linear TMD becomes detuned due to disturbances, such as potential degradation of structural stiffness (Pinkaew *et al*. 2003, Sgobba and Marano 2010). Additionally, TMDs are reported to experience excessive working stroke, especially in towering structures or high-rise buildings where mounting space at the top is limited (Zuo and Zhu 2022). To address these problems, advanced TMDs integrated nonlinear components are developed, such as particle tuned mass damper (Lu *et al*. 2022), gas-spring dynamic vibration absorber (DVA) (Rong and Lu 2021, 2022, Rong *et al*. 2023), inerter-based TMD (Ma *et al*. 2021, Zuo *et al*. 2021), etc. Advanced materials such as shape memory alloys (SMAs) have also been introduced to the vibration reduction fields, and the underlying principle of the materials could offer illumination on addressing the aforementioned issue.

Reversible phase transitions in SMAs result in their distinctive characteristics, which can be categorized as the shape memory effect (SME) and the superelastic effect (SE) (Ghasemi *et al*. 2019). The SME refers to the ability of SMAs to revert to their predefined shape even when subjected to substantial strain (up to 10%) upon heating, while SE denotes the capability of SMAs to withstand significant inelastic deformations and subsequently recover their original shapes after unloading (Song *et al*. 2006). SMAs have gained prominence in diverse domains, owing to their fatigue resistance, enduring durability, and superior damping capabilities compared to other rubber or elastomeric materials. When incorporated into vibration control of civil structures, SMAs can function as passive, semi-active, or active elements to mitigate harmful

*Corresponding author, Ph.D. Student,
E-mail: myaozhou@163.com
[a] Ph.D.
[b] Ph.D. Student
[c] Ph.D.

ISSN: 1738-1584 (Print), 1738-1991 (Online)

oscillations.

Some researchers employed the particular thermomechanical properties of SMA dedicated to actively controlling the vibration by thermal activation of SMA (Rustighi *et al*. 2005a, Belyaev *et al*. 2014, Santos and Nunes 2017, Berardengo *et al*. 2019). Huang *et al*. (2017) explored the dynamic traits of SMA spanning temperatures from 11°C to 120°C, and conducted experiments to mitigate vibrations of timber floor (Huang *et al*. 2017, Huang and Chang 2018) and steel frame structure (Huang *et al*. 2020). Results show that the effectiveness of heating SMA-based TMDs is often restricted due to minor changes in dynamic properties at temperatures above 19°C. Manzoni *et al*. (2023) compared two layouts of SMA, i.e., wire-based and beam-based, in the damper and assessed their mechanical performance. Results suggest that as the required eigenfrequency rises, the size of the wire-based TMD may become too small in size to serve in practice. Moreover, some research has exwlored SMA-based dampers incorporating SMA beam elements (Williams *et al*. 2002, Rustighi *et al*. 2005b), SMA rod (Wang and Melnik 2012), SMA-inerter assemblies (Das *et al*. 2021a, Tiwari *et al*. 2021), SMA pendulum (Contreras *et al*. 2014, Pasala and Nagarajaiah 2014) or SMA spring (Mani and Senthilkumar 2015), concerning thermo-mechanical coupling. The results indicate that dampers integrating SMA as a tuning component hold promise as a simple and high-performance approach for vibration mitigation. Rather than solely relying on SMA, Berardengo *et al*. (2015) devised an adaptive tuned mass damper, combining SMA and eddy currents. Kumbhar *et al*. (2018) proposed an adaptive TVA using magnetorheological elastomer-shape memory alloy composite.

In the above-mentioned research, temperature-based control methods employing SMA are established and proven effective. However, these dampers exhibit long response time due to thermal inertia, strong nonlinearity in tuning parameters dependent on current, and inefficient energy conversion activated by electrical signals. For example, the complete transformation in literature (Rustighi *et al*. 2005b) takes about 120 s using a 9 A current to heat the SMA wire. Additionally, detecting changes in the material state is challenging, and usually requires the use of complicated control systems (Rustighi *et al*. 2005b, Huang *et al*. 2017). Consequently, difficulties remain in the practical implementation of SMA's thermo-mechanical coupling properties, particularly within civil engineering structures where the size of SMA components is substantial and the aforementioned limitations become more prominent.

By fully leveraging the SE of SMA, the SMA-based elements, with notable energy dissipation capacity through hysteresis phase transformation under cyclic loading, are utilized to serve in gap damper of isolation systems (De Domenico *et al*. 2020, De Domenico and Gandelli 2021), reduce the excessive loads on the perimeter column in timber buildings (Das and Tesfamariam 2022), suppress excessive vibrations of bridge deck (Liu *et al*. 2017), bridge cables (Dieng *et al*. 2013, Torra *et al*. 2014)and wind turbine tower (Zuo *et al*. 2022). Furthermore, SMAs are employed as a substitute for linear spring elements in passive vibration control devices, called SMA-TMD or SMA-TVA. Mishra *et al*. (2013) numerically compared the SMA-TMD and traditional linear TMD in mitigating seismic vibrations of structures. The results showed that SMA-TMD significantly improves control efficiency while requiring a reduced working stroke. At the same level of control efficiency, SMA-TMD has a substantially lower required mass ratio compared to the linear TMD. Lv and Huang (2023b) tested a nonlinear TMD with pre-strained SMA helical springs on a single-layer structure and observed that structural vibrations can be effectively suppressed, even with a detuning ratio of 15%. Gur *et al*. (2014) utilized an SMA spring to tune a liquid column damper and found that the damper can control broad-band earthquake-induced vibrations in relatively short-period structures. Tian *et al*. (2019, 2020) investigated the efficacy of SMA-TMD in controlling vibrations in transmission tower-line systems and found that seismic demand mitigation is always attained across a broad temperature range typical for engineering applications. Das *et al*. (2021b) introduced an SMA-assisted nonlinear energy sink (NES) incorporating negative stiffness and sliding friction.

Previous studies have shown that the coil-type SMA springs are capable of achieving a significantly larger displacement, exceeding 100% of its initial length, thereby enabling broader applications compared to the wire-type SMA actuator, which is limited to generating a displacement of less than 6–8% of its original length (Koh 2018). Hence, this study focuses on SMA-TVA, which entails substituting the linear springs in conventional TVA with superelastic coil-type SMA springs for structural vibration mitigation. Despite substantial research on the performance of SMA-based dampers, there is still a scarcity of experimental validation for SMA-TVA in the vibration control of multi-degree-of-freedom (MDOF) structures, particularly regarding the evolution of time-frequency energy under different incentives and variations of SMA effects under parameter deviations. In this study, Nitinol SMA is chosen for the fabrication of SMA specimens, and cyclic displacement loading tests are performed on both SMA wire and spring. Shaking table tests are then designed and executed on a three-story steel shear frame controlled by SMA-TVA and conventional linear TVA, respectively. The superiority and robustness of SMA-TVA are validated, covering multi-layer responses of the structure in both time and frequency domains under various seismic excitations, different excitation amplitudes, and different frequency ratios.

2. Hysteresis of SMA

SMAs are promising smart materials to form robust hysteretic dampers with wide frequency bandwidth and enhanced vibration absorption. These materials are capable of changing their modulus under the influence of external stimuli and temperature, leading to their merit of superelasticity and outstanding re-centering capabilities (Das *et al*. 2021a). To date, numerous varieties of SMAs

have been identified and certain recently introduced SMAs cost much less (Tiwari *et al*. 2021). In terms of vibration suppression technology, Nitinol SMA, specifically the Ni-Ti alloy, boasts superior thermomechanical and thermoelectrical characteristics than copper and steel counterparts and stands as the predominant SMA choice (Song *et al*. 2006).

Fig. 1 illustrates the typical stress-strain-temperature behavior of the SMA (Mirzai *et al*. 2021). SMA possesses the transformation between two distinct crystalline phases: low- and high-temperature stable phases, i.e., martensite and austenite phases. The prevalent phase within the alloy is contingent upon temperature and stresses and is dictated according to its chemical composition and the thermodynamic transformations during its fabrication. Notably, martensite, characterized by a parallelogram structure, exhibits relative weakness and susceptibility to deformation, whereas austenite, with its body-centered cubic crystal structure, demonstrates greater resistance to external stresses. The transformation between different crystal phases defines the unique properties of SMAs, namely SME and SE. SME is a thermally induced phase transformation phenomenon. As seen in Fig. 1, it occurs when an SMA in the low-temperature martensitic phase. After undergoing a certain degree of deformation, SMA can recover its original shape upon heating above the martensite-to-austenite phase transition temperature ($T > A_f$). SE, on the other hand, is a phenomenon that occurs in the high-temperature austenitic phase. SMAs can exhibit large, reversible strains under significant applied stress, and this process can occur at a constant temperature. Specifically, when $T > A_f$, the SMA is in the high-temperature austenitic phase. Applying stress induces a stress-driven phase transformation from the austenitic to the martensitic phase. Once the stress is removed, the material undergoes a reverse phase transformation from martensite back to austenite, returning to its original austenitic structure, forming a closed loop in the stress-strain curve.

Utilizing the SE of SMA, an SMA-TVA is introduced in this study to mitigate structural vibrations under earthquakes, integrating the vibration control mechanism of a conventional TMD and the energy dissipation of SMA springs. The schematic diagram of the SMA-TVA system is presented in Fig. 2. The SMA-TVA includes a mass block connected to a box using SMA springs, with the box securely attached to the location of maximum structural vibration (the top floor of the structure in this study). The assembly incorporates mechanical components like wheels or tracks to facilitate sliding within the box, and it is assumed frictionless for sliding.

The SMA spring is primarily characterized by a coil diameter D and wire diameter d, as illustrated in Fig. 2. The relationship governing the parameters related to the shape of the SMA spring is expressed as follows

$$D = \left(\frac{Ed^4}{16nk(1+\nu)}\right)^{\frac{1}{3}} \tag{1}$$

where E, ν, and k represent the elastic modulus, Poisson's ratio, and lateral stiffness of the spring. n represents the number of spring coils.

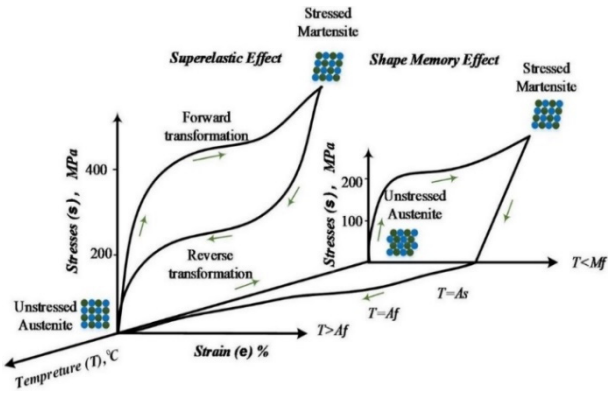

Fig. 1 Typical stress-strain-temperature behavior of the SMA (Mirzai *et al*. 2021)

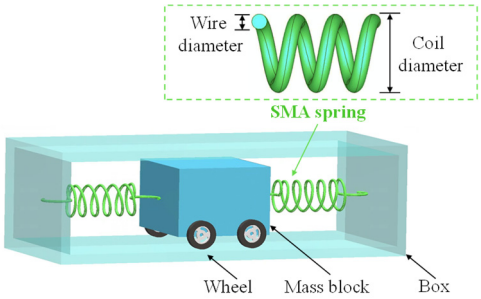

Fig. 2 Schematic diagram of SMA-TVA system

The primary goal of this study is to experimentally compare and validate the vibration reduction performance of SMA-TVA relative to traditional TVA. Therefore, the tuning parameters for SMA-TVA are calculated using the methodology employed for traditional TVA (Den Hartog 1947)

$$k = m(2\pi f_0)^2 {f_{\text{opt}}}^2 \tag{2}$$

$$f_{\text{opt}} = 1/(1+\mu_m) \tag{3}$$

where f_0 is the natural frequency of the controlled structure. m is the mass of the mass block in the damper. f_{opt} and μ_m are optimal frequency ratio and mass ratio of the damper to the structure, respectively. For simplicity, all frequency ratios discussed in the following text are expressed as ratios to f_{opt}.

Prior to the shaking table tests that comprised the complete controlled structure, loading tests on SMA material and element were carried out. According to previous research (Qiu *et al*. 2018, Tian *et al*. 2020, Moraes *et al*. 2023), Ni-Ti alloy exhibits good hysteresis performance. Therefore, in this study, Ni-Ti alloy is selected as the spring material in the SMA-TVA. The diameter and gauge length of the tested Ni-Ti wires are 0.6 mm and 140 mm, respectively. The coil diameter and gauge length of the Ni-Ti based springs are 10.6 mm and 8 mm, respectively, corresponding to the optimal frequency ratio f_{opt}. All specimens underwent testing under room temperature conditions and in austenitic states. The mechanical characteristics of the materials were assessed utilizing an

(a) History (b) Strain-stress

Fig. 3 Cyclic displacement loading of the SMA wire

(a) History (b) Displacement-force

Fig. 4 Cyclic displacement loading of the SMA spring

electronic universal testing machine (WDW-100) with a capacity of 100 kN and a precision for tensile displacement of up to 0.001 mm. The cyclic testing of the SMA specimens employed the displacement control method. where displacement was measured by a displacement sensor, and load was recorded by the load sensor in the testing apparatus. The cyclic loading procedure and recorded results are depicted in Figs. 3 and 4, wherein the strain amplitude incrementally rises by 1% for SMA wire and 40% for SMA spring. It should be noted that the initial length of the test spring is extended to match the length used in subsequent testing on the vibration table institutions.

From Figs. 3 and 4, it is seen that the SMA material exhibits apparent superelasticity. The superelastic Ni-Ti wire demonstrates a singular plateau during both loading and unloading sequences. Exceeding a critical stress threshold during loading triggers the activation of austenitic to martensite phase transformation, resulting in the emergence of a stress plateau. Upon unloading, the martensite undergoes instability and transforms back to austenite along a lower-stress plateau. Furthermore, the presence of a higher stress plateau at substantial strain levels offers advantages for effective deformation control in the context of heightened seismic intensity conditions. The peak superelastic strain amplitude of the Ni-Ti wire is approximately 10%, beyond which the complete recovery of deformation may not occur, leading to the presence of noticeable residual strain. Consequently, the Ni-Ti SMA wire, possessing a superior elastic strain amplitude compared to steel material, can maintain its seismic-resistant capability and minimize structural permanent deformation following intense earthquakes when appropriately incorporated into seismic-resistant structures.

3. Shaking table test setup

3.1 Test model

The shaking table test was carried out using a three-story steel shear frame, as shown in Fig. 5. The bottom of the steel frame is fixed to the shaking table, which can provide a maximum acceleration of 24.5 m/s^2 and a maximum travel distance of ±7.5 cm. The length, width and height of each layer of the structure model are 300 mm, 120 mm and 200 mm, respectively. The total mass of the model is 13.87 kg, including the mass of base for fixing the damper and the mass of acceleration sensors. Four acceleration sensors were mounted on top of each floor and the base of the structure. Three laser displacement sensors were mounted on a shelf to collect displacement data of the 2nd and 3rd floors of the structure and the damper mass block, respectively. Before the test, white noise scanning is

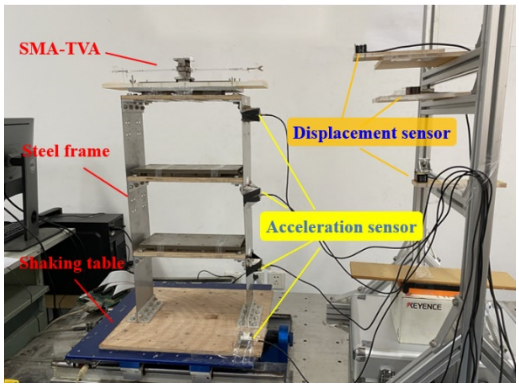

Fig. 5 Experimental structure with damper

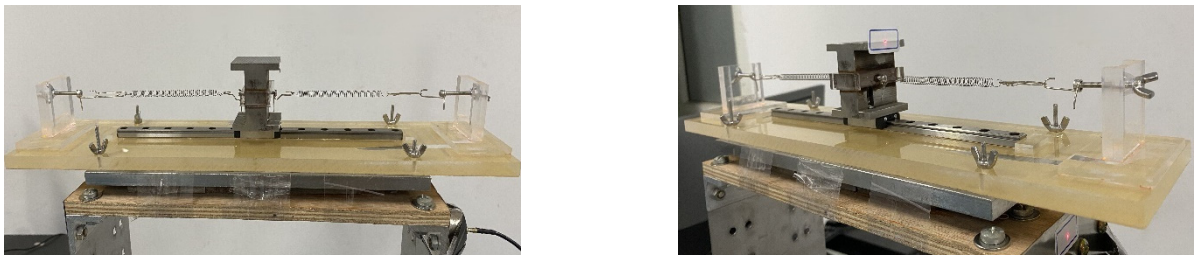

(a) Front view (b) Side view

Fig. 6 Experimental photos of SMA-TVA

conducted to obtain the dynamic characteristics. The damping ratio of the steel frame tested through free decay vibration tests is 0.01, and the natural frequencies of the first three modes are 1.95 Hz, 5.67 Hz and 7.81 Hz, respectively. Fig. 6 shows the close-up photos of the designed SMA-TVA device utilized in the test. The damper is mounted on the top of the steel frame, and the end plates are arranged on the mass block rail to prevent the damper. The damper mass block weighs 0.346 kg, which corresponds to a mass ratio to the structure of about 2.5%. In the optimal tuning conditions, the stiffness of each spring in the damper is approximately 20 N/m.

3.2 Test condition design

Table 1 presents the designed test conditions with the main parameters. The experiment began with the free vibration, featuring an initial displacement of 20 mm (A1 in Fig. 7), of the three-story frame to preliminarily assess the damping effect of SMA-TVA. Subsequently, shaking table tests for the frame structure were carried out with different control methods (uncontrolled, TVA control and SMA-TVA control) under resonant harmonic excitation (A2) and seismic excitations (B1~B4), respectively. It should be noted that the tuning parameters of the springs in TVA are identical to those in the SMA-TVA. Four seismic waves are selected as inputs to compare the performance of two dampers under different seismic excitations. Fig. 7 illustrates the time history and spectrum of the selected seismic waves. The peak ground acceleration (PGA) of each seismic excitation is adjusted to 0.05 g except for AWX wave (B4). This is because the response of the structure at 0.05 g is excessive for this seismic wave, so its PGA is adjusted to 0.02 g. Finally, C1~C7 and D1~D4 were designed to investigate the performance variation of SMA-TVA under different excitation amplitudes and different frequency ratios, respectively.

4. Free vibration and harmonic excitation

Fig. 8 illustrates the time histories of the top-floor displacement of the steel shear frame structure at an initial displacement of 20 mm during free vibration. It can be observed that the structure nearly comes to a standstill after about 7 s under SMA-TVA control, whereas without control, the structure persists in experiencing notable oscillations. The results suggest that the SMA-TVA can effectively and promptly suppress structural vibrations.

Fig. 9 illustrates the dynamic acceleration and displacement responses of the structure at the top floor under resonant harmonic excitation with an amplitude of 1 mm. After approximately 40 s, the excitation ceases, and the structure enters a state of free vibration. It is apparent from the figure that both the TVA and SMA-TVA successfully reduce the dynamic response of the structure. In terms of TVA control, the acceleration and displacement responses of the structure in about the first 15 s are greater than those after the structure enters steady-state motion (30-40 s). In contrast, the initial increase in the structural response under SMA-TVA control is not obvious. This suggests that SMA-TVA enhances the overall damping of the system, effectively reducing its transient response and facilitating a quicker transition to the steady-state motion stage. During the period of structural free vibration, it is evident that under SMA-TVA control, the structure comes to a complete

Table 1 Test conditions

No.	Test condition	Excitation type	Wave name	Frequency ratio	PGA (g)
1	A1	Initial displacement of 20 mm	/	/	/
2	A2	Harmonic excitation	/	1.0	/
3	B1	Seismic excitation	Northridge	1.0	0.05
4	B2		El Centro	1.0	0.05
5	B3		Imperial Valley	1.0	0.05
6	B4		AWX0.9-2	1.0	0.02
7~13	C1~C7		Northridge	1.0	0.02, 0.04, 0.06, 0.08, 0.10, 0.12, 0.14
14~17	D1~D4		Northridge	0.778, 0.875, 1.157, 1.27	0.10

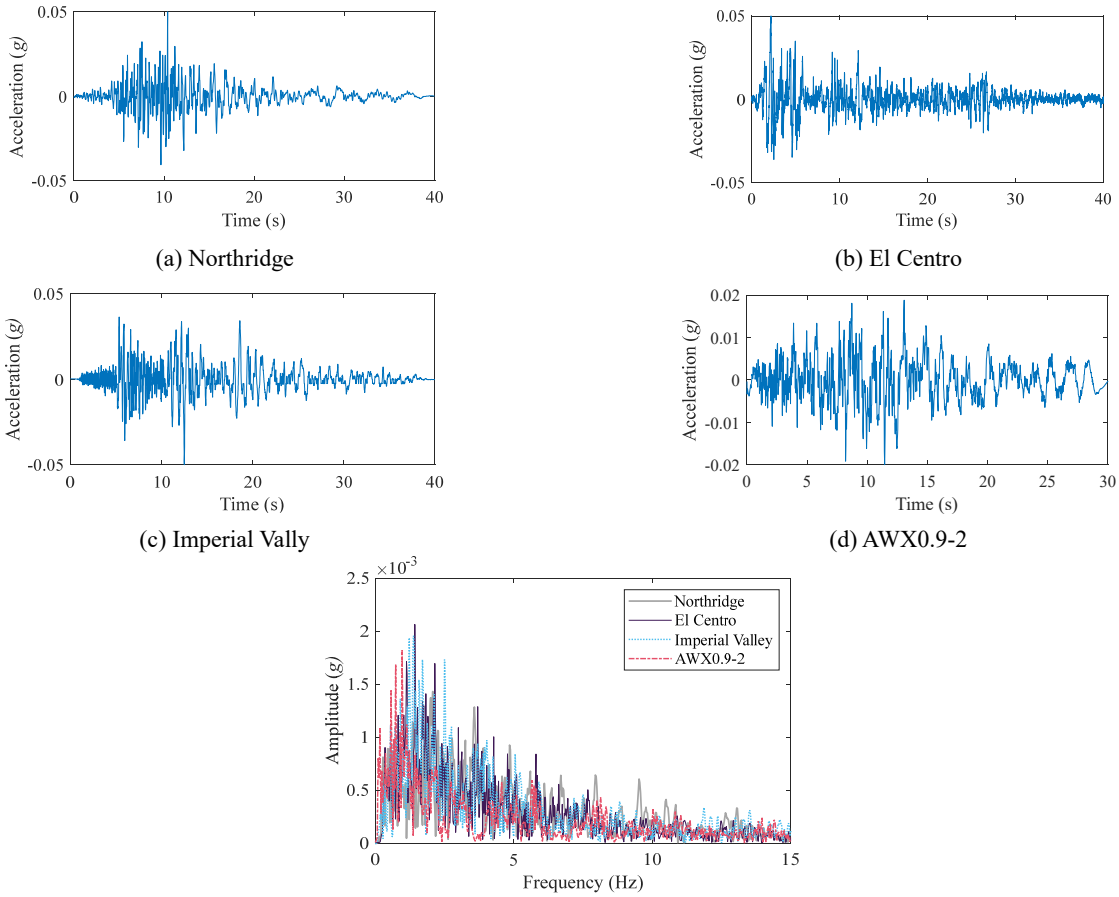

(a) Northridge (b) El Centro

(c) Imperial Vally (d) AWX0.9-2

(e) Spectrum

Fig. 7 Time history and spectrum of the seismic waves in the experiment

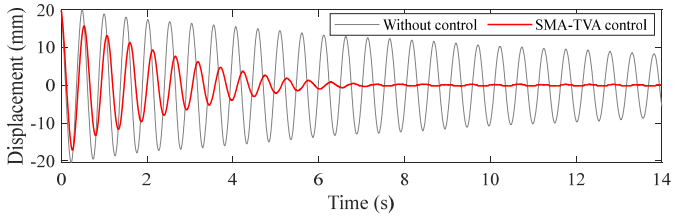

Fig. 8 Top-floor displacement response of structure at an initial displacement of 20 mm

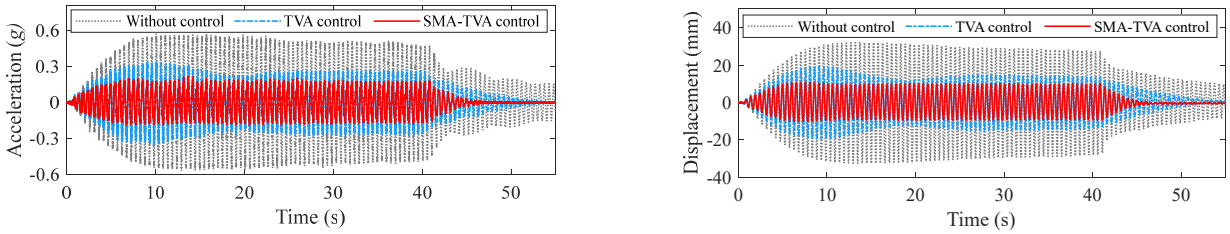

(a) Top-floor acceleration (b) Top-floor displacement

Fig. 9 Dynamic response of structure under harmonic excitation

stop in approximately 5 s, whereas under TVA control, it takes about 15 s. These observations suggest that SMA-TVA enhances the control effects of structural response and operates more swiftly than TVA, with more consistent damping performance throughout the entire time course.

Fig. 10 presents the motion of the damper, i.e., the displacement of mass block relative to the structure. It is seen that the SMA-TVA maintains a more stable motion and has a smaller stroke than TVA. By substituting the normal spring with an SMA spring, the maximum stroke of the

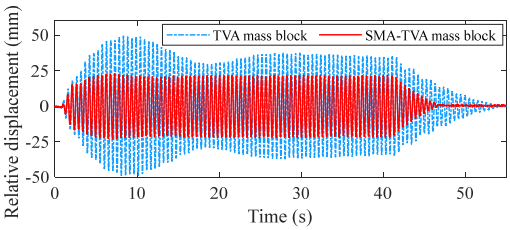

Fig. 10 Time histories of the displacement of damper relative to structure

damper can be reduced by 54.3% from 49.4 mm to 22.6 mm.

5. Seismic vibration mitigation of SMA-TVA

In order to comprehensively and objectively validate the performance of SMA-TVA under seismic excitations, this section presents the results of multiple shaking table test conditions. The study of the effectiveness and robustness of SMA-TVA includes multi-layer responses of structure under various seismic excitations, different excitation amplitudes, and different frequency ratios.

5.1 Performance under various earthquakes

To explore the damping performance of SMA-TVA under unpredictable seismic excitation, the displacement histories of the structure at the top floor without and with control under various seismic waves are illustrated in Fig. 11. It can be observed that the displacement responses of the structure are generally reduced by the TVA and SMA-TVA compared with the uncontrolled structure. It is noticeable that at a few moments during vibration (around 25 s in Fig. 11(e) and 20 s in Fig. 11(g)), TVA amplifies the displacement response of the structure, whereas SMA-TVA realizes an effective control of structural response. This superiority of SMA-TVA is not restricted to a specific seismic excitation, demonstrating that the SMA-TVA can prevent the structural safety against hazardous earthquake events.

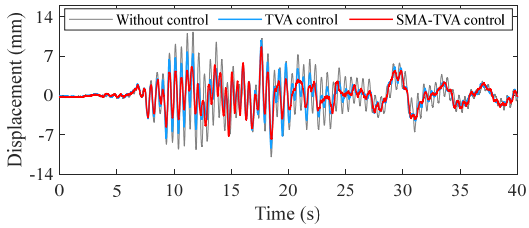

(a) B1 displacement

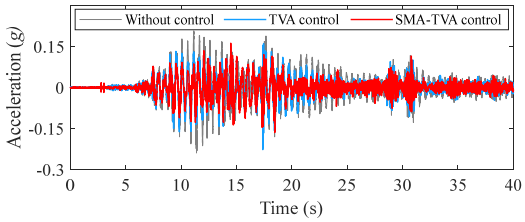

(b) B1 acceleration

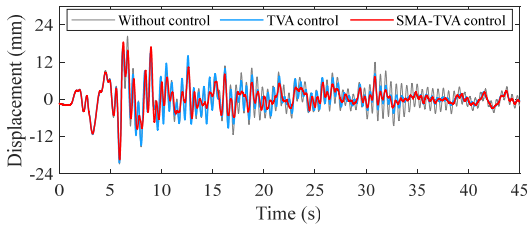

(c) B2 displacement

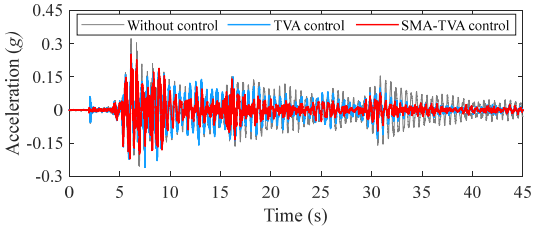

(d) B2 acceleration

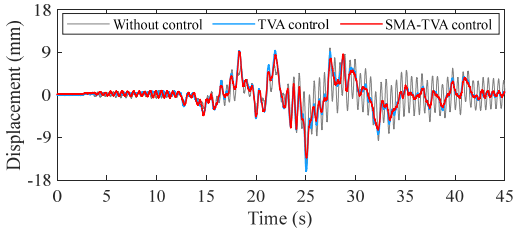

(e) B3 displacement

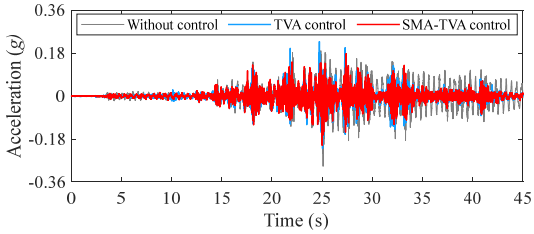

(f) B3 acceleration

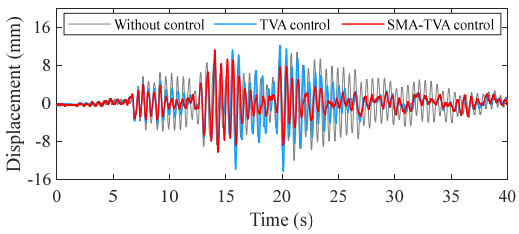

(g) B4 displacement

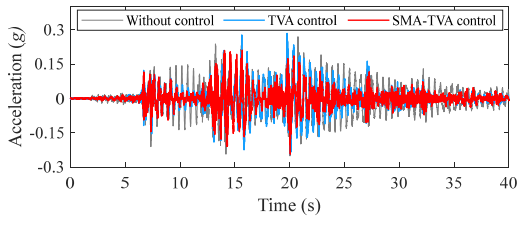

(h) B4 acceleration

Fig. 11 Top-floor times histories of the structure under various seismic motions

Table 2 Reduction ratios of two dampers and improvement rates of SMA-TVA relative to TVA

Test condition	Displacement reduction ratio (%)				Acceleration reduction ratio (%)				Improvement rate (%)				Stroke
	Peak		RMS		Peak		RMS		Displacement		Acceleration		
	TVA	SMA-TVA	TVA	SMA-TVA	TVA	SMA-TVA	TVA	SMA-TVA	Peak	RMS	Peak	RMS	
B1	13.2	23.7	24.7	35.2	5.3	31.4	31.8	43.7	79.8	42.4	491.2	37.5	29.5
B2	2.2	6.6	9.3	19.4	19.5	21.4	22.2	41.2	193.2	107.7	9.9	85.2	25.4
B3	-19.3	6.2	18.7	39.1	-5.6	9.5	22.9	39.4	/	109.3	/	72.2	42.5
B4	-9.9	9.4	0.77	9.5	21.9	29.8	42.3	44.8	/	/	36.4	6.0	11.6

*Note: "/" indicates that the vibration reduction rate of TVA is negative or too small to obtain a reasonable improvement rate

Table 2 lists the reduction ratio of the dampers, i.e., the ratio of the change in the structure's response when controlled to the original uncontrolled response. Regarding the control effects on structural displacement at the top floor, two dampers present better vibration mitigation effects under B1, where TVA and SMA-TVA present up to 24.7% and 35.2% RMS reduction ratio, respectively. The improvement rates for peak and RMS displacement control for this case are 79.8% and 42.4%, respectively. For other cases, the advantages of SMA-TVA over TVA are more clearly demonstrated, especially for B3 and B4 where TVA is not helpful for peak displacement damping rates. In terms of structural acceleration reduction, the ratios of peak acceleration for the top floor under TVA and SMA-TVA control are 5.3% and 31.8% under Northridge wave (B1). SMA-TVA achieves up to 109.3% and 85.2% improvement in RMS displacement and acceleration reduction effects, respectively, compared to TVA. The experimental results indicate that SMA-TVA exhibits superior stability and insensitivity under random excitations compared to its counterpart, the TVA with linear steel springs only.

The differences in control performance between TVA

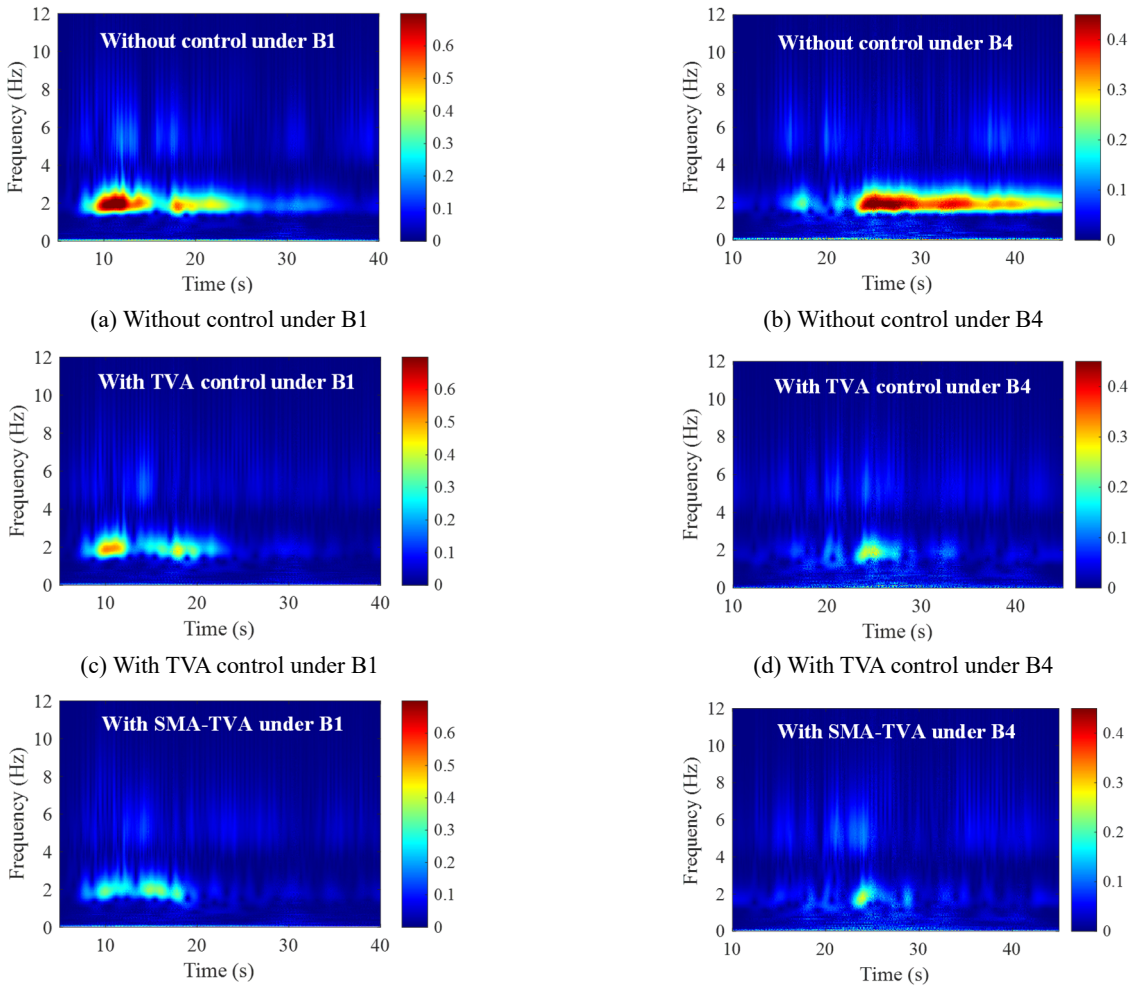

(a) Without control under B1

(b) Without control under B4

(c) With TVA control under B1

(d) With TVA control under B4

(e) With SMA-TVA control under B1

(f) With SMA-TVA control under B4

Fig. 12 Top-floor acceleration time-frequency energy under different seismic motions under B1 or B4

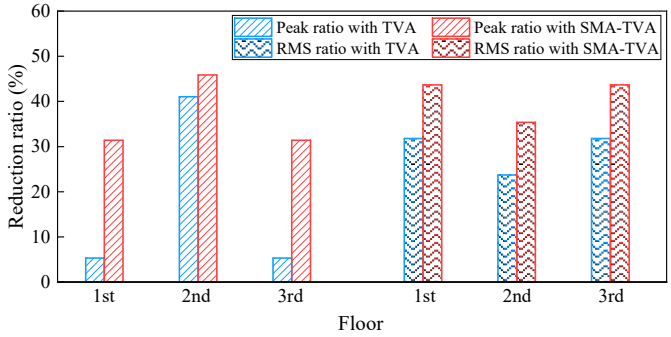

Fig. 13 Acceleration reduction ratio of each floor with TVA or SMA-TVA

and SMA-TVA under diverse seismic excitations can be explained by the wavelet analysis. Fig. 12 plots the acceleration time-frequency energy of the structure in terms of Northridge wave (B1) and AWX wave (B4) as examples. The time-frequency energy spectra are obtained using continuous wavelet transform (CWT), providing a representation of the frequency variation in the structural acceleration response over time. The distribution of structural vibration energy can be discerned in both the time and frequency domains, with color indicating the magnitude of energy. As depicted in Figs. 12(a) and (b), the structural vibrations without control are predominantly concentrated at 1.96 Hz, corresponding to the first natural frequency of the primary structure. The energy of the uncontrolled structures differs in time distribution under the two seismic wave inputs. Specifically, the AWX wave sustains a prolonged period of high energy input compared to the Northridge wave. In this scenario, the damper can maintain a higher level of vibration, as illustrated in Figs. 11(g)~(h), with a significant portion of energy transferring from the structure to the damper. This facilitates more efficient and stable attenuation of vibrations, as observed in Figs. 12(d) and (f), where vibrations are confined within a shorter duration compared to Figs. 12(c) and (e). In addition, SMA-TVA is able to accelerate the energy dissipation of the structure relative to TVA. This phenomenon leads to greater reduction effects of structural responses under SMA-TVA control, which is consistent with the acceleration reduction ratios shown in Table 2.

To analyze the control efficiency of SMA-TVA on different floors of the MDOF structure, the acceleration reduction ratio of each floor under the control of TVA and SMA-TVA is compared in Fig. 13. It can be seen that SMA-TVA achieves effective attenuation on structural acceleration response of each floor, but the control efficiency of TVA on the 1st and 3rd floors is not obvious. Fig. 14 further presents the acceleration spectra of each floor of the structure employing different dampers. It is observed that under Northridge wave (B1), the acceleration responses of the 2nd and 3rd floors of the uncontrolled

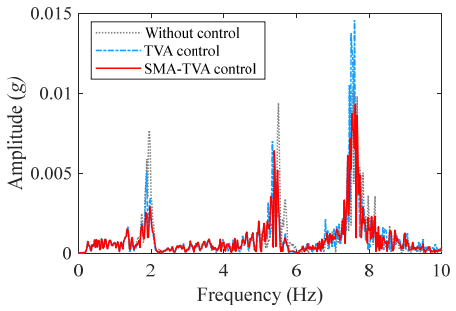

(a) 1st floor

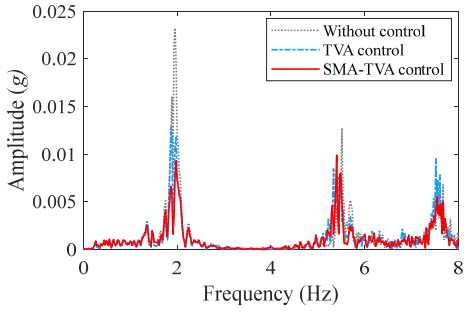

(b) 2nd floor

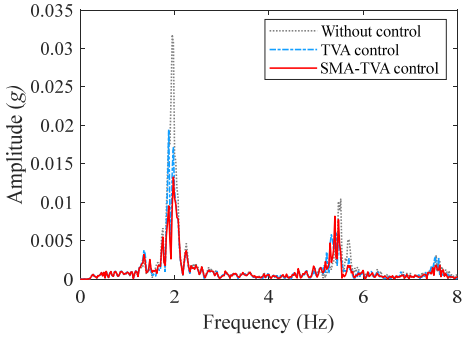

(c) 3rd floor

Fig. 14 Acceleration response spectra of different floors under B1

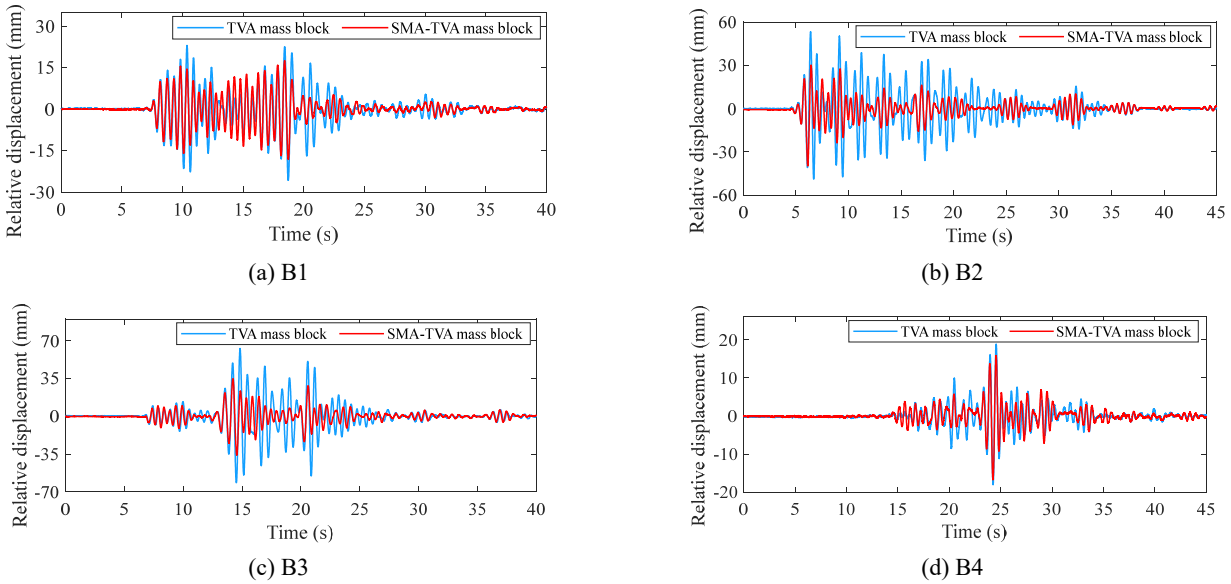

(a) B1 (b) B2

(c) B3 (d) B4

Fig. 15 Displacement time histories of dampers under various seismic motions

structure are primarily concentrated around the first-order frequency, while the acceleration response of the 1st floor is mainly distributed around the third-order frequency. Both TVA and SMA-TVA demonstrate effectiveness in reducing first-order vibrations across all three floors. However, when it comes to the activated third-order mode vibration, particularly in the response of the first floor, TVA proves counterproductive, amplifying the motion of the mode significantly. This amplification is unfavorable for vibration mitigation. The damping effect of SMA-TVA extends beyond its tuning frequency, effectively dissipating energy associated with multiple modes through the hysteresis feature of the SMA spring. This characteristic results in the stable damping effect of SMA-TVA.

Fig. 15 compares the strokes of TVA and SMA-TVA, i.e., the absolute displacement of the mass block in the damper relative to the top-floor displacement response of the structure. The time-course curves reveal that SMA-TVA exhibits a notable stroke advantage over TVA, particularly when structural response is substantial and movement amplitude of TVA increases. For instance, in Fig. 15(c), the TVA stroke is the largest among the four seismic excitations, reaching nearly 70 mm. In this scenario, the SMA-TVA stroke is notably reduced to a greater extent. Additionally, the quantitative data in Table 2 indicates that the stroke of SMA-TVA can be decreased by up to 42.5% (under B3).

5.2 Excitation amplitude

Fig. 16 illustrates the vibration reduction ratio of structural acceleration and displacement responses under Northridge wave with varying PGA while keeping the frequency ratio, mass ratio, and other parameters unchanged. It is noticeable that when PGA is 0.02 g, the damping performance of TVA and SMA-TVA is comparable. This similarity arises because, the structural movement is limited under smaller amplitude excitations, leading to a low-magnitude displacement of the mass block in the damper. In this condition, the SMA spring operates in a linear stage, behaving similarly to a conventional steel spring, thereby resulting in comparable performance with TVA.

As PGA increases, the performance disparity between the two dampers becomes progressively evident, with similar trends in the changes in performance. When PGA reaches 0.14 g, both dampers experience a degradation in damping effects. This is attributed to the excessive strokes of the dampers observed in the tests, indicating that their physical configurations are inadequate for the required strokes. Even with this degradation in performance, SMA-TVA generally exhibits better damping efficiency than TVA, suggesting that SMA-TVA can maintain its effectiveness under high-intensity excitation.

Table 3 lists the reduction ratios of two dampers under various excitation amplitudes. The quantitative results reveal that the control performance of the structural dynamic responses can be enhanced by up to approximately 38%, and the working stroke can be optimized by up to 40% through the implementation of SMA-TVA.

5.3 Tuning frequency ratio

Recognizing that the natural frequency of the structure may deviate due to factors such as structural damage or changes in environmental conditions, this section explores various frequency ratios of the damper. The experiment utilizes four frequency ratios under the Northridge wave with an intensity of 0.10 g, spanning 0.778, 0.875, 1.157, to 1.270, with a constant frequency ratio condition used for comparison. The variation of tuning frequency ratios in the tests is achieved by replacing SMA springs with different stiffnesses. Fig. 17 shows the reduction ratios of structural responses under SMA-TVA control with the specified frequency ratios. The results indicate that SMA-TVA effectively attenuates structural acceleration and displacement responses under seismic excitation across all the examined frequency ratios. For the frequency ratios at

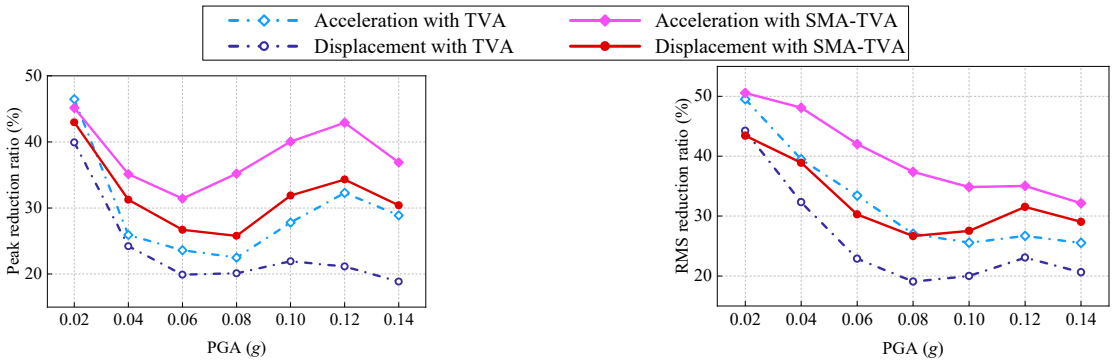

(a) Peak reduction ratio (b) RMS reduction ratio

Fig. 16 Reduction ratios of structural responses with different PGA

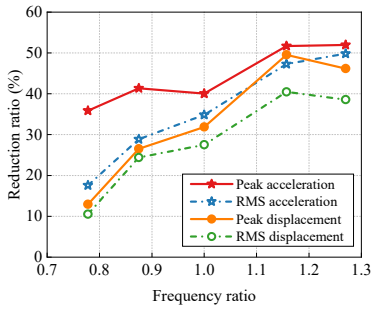

Fig. 17 Reduction ratios of structural response under SMA-TVA control with different frequency ratios

the extremes of the investigated cases (0.778 and 1.270), the average change in the vibration reduction ratio is 13.7%, suggesting that SMA-TVA exhibits robustness against tuning frequency deviation. It's worth noting that the attenuation efficiency of SMA-TVA performs better by increasing the tuning frequency ratio. This phenomenon is attributed to the nonlinear deformation of the SMA spring. As the SMA spring surpasses its linear stage and enters the nonlinear stage, its stiffness decreases, resulting in a reduction in the frequency ratio. Due to this internal nonlinear behavior of the SMA spring, when SMA-TVA is initially designed to have a higher tuning frequency ratio, the deformation of the SMA spring tends to bring the damper closer to the inherent frequency of the structure and perform better control effects.

6. Conclusions

This study employs the superelastic SMA-TVA to control the seismic vibrations of MDOF structures. Shaking table tests are conducted on a three-story steel shear frame. The effectiveness and robustness of SMA-TVA are validated, covering multi-layer responses of the structure in both time and frequency domains under various seismic excitations, different excitation amplitudes, and different frequency ratios. The main conclusions drawn from the experiments are as follows:

- SMA-TVA demonstrates superior stability and insensitivity, particularly in controlling activated third-order mode vibration on the first floor. Unlike counterproductive TVA, SMA-TVA effectively attenuates vibrations beyond its tuning frequency, dissipating energy associated with multiple modes. It outperforms TVA with a significant 109.3% and 85.2% improvement in RMS displacement and acceleration reduction, respectively, with strokes reduced by up to 42.5% under earthquakes.
- The differences in control performance between TVA and SMA-TVA under various diverse excitations are investigated through time-frequency energy analysis. Certain earthquakes exhibit a prolonged period of high energy input, allowing the damper to maintain a higher level of vibration. Consequently, a substantial portion of energy is

Table 3 Reduction ratios of two dampers under various excitation amplitudes

Test condition	Displacement reduction ratio (%)				Acceleration reduction ratio (%)				Improvement rate (%)				Stroke
	Peak		RMS		Peak		RMS		Displacement		Acceleration		
	TVA	SMA-TVA	TVA	SMA-TVA	TVA	SMA-TVA	TVA	SMA-TVA	Peak	RMS	Peak	RMS	
C1	49.5	50.6	44.2	43.4	46.5	45.2	39.9	43.0	2.1	-1.9	-2.9	7.0	18.2
C2	39.5	48.1	32.3	38.9	25.9	35.1	24.2	31.2	17.9	17.0	26.2	22.5	27.9
C3	33.4	42.0	22.9	30.3	23.6	31.4	19.9	26.7	20.5	24.4	24.9	25.5	24.6
C4	27.0	37.4	19.1	26.7	22.5	35.2	20.1	25.8	27.7	28.6	36.1	22.1	36.0
C5	25.6	34.8	20.0	27.5	27.8	40.0	21.9	31.9	26.6	27.4	30.6	31.2	36.3
C6	26.7	35.0	23.1	31.5	32.3	42.9	21.1	34.3	23.8	26.9	24.8	38.4	39.9
C7	25.5	32.2	20.6	29.0	28.9	36.9	18.9	30.4	20.6	29.0	21.8	38.0	38.7

transferred from the structure to the damper, facilitating more efficient and stable attenuation of vibrations.

- When the excitation amplitude is small, the SMA spring operates in a linear stage, behaving similarly to a conventional steel spring. As PGA increases, the performance disparity between the two dampers becomes progressively evident, with SMA-TVA demonstrating effectiveness even under high-intensity excitation. The average change in the vibration reduction ratio remains below 13.7% within the considered varying frequency ratios, indicating that SMA-TVA exhibits robustness against tuning frequency deviation.

Acknowledgments

Financial supports from National Natural Science Foundation of China (No. 52308509) are highly appreciated. This work is also supported by China Postdoctoral Science Foundation under Grant Number 2023M742096.

References

Belyaev, A.K., Irschik, H. and Krommer, M. (2014), *Mechanics and model-based control of advanced engineering systems*, Springer Vienna.

Berardengo, M., Cigada, A., Guanziroli, F. and Manzoni, S. (2015), "Modelling and control of an adaptive tuned mass damper based on shape memory alloys and eddy currents", *J. Sound Vib.*, **349**, 18-38. http://doi.org/10.1016/j.jsv.2015.03.036

Berardengo, M., Della Porta, G.E.P., Manzoni, S. and Vanali, M. (2019), "A multi-modal adaptive tuned mass damper based on shape memory alloys", *J. Intell. Mater. Syst. Struct.*, **30**(4), 536-555. http://doi.org/10.1177/1045389X18818388

Contreras, M.T., Pasala, D.T.R. and Nagarajaiah, S. (2014), "Adaptive length SMA pendulum smart tuned mass damper performance in the presence of real time primary system stiffness change", *Smart Struct. Syst., Int. J.*, **13**(2), 219-233. http://doi.org/10.12989/sss.2014.13.2.219

Das, S. and Tesfamariam, S. (2022), "Multiobjective design optimization of multi-outrigger tall-timber building: Using SMA-based damper and lagrangian model", *J. Build. Eng.*, **51**, p. 104358. http://doi.org/10.1016/j.jobe.2022.104358

Das, S., Chakraborty, A. and Barua, I. (2021a), "Optimal tuning of SMA inerter for simultaneous wind induced vibration control of high-rise building and energy harvesting", *Smart Mater. Struct.*, **30**(2), p. 025027. http://doi.org/10.1088/1361-665X/abd42a

Das, S., Chakraborty, S., Chen, Y. and Tesfamariam, S. (2021b), "Robust design optimization for SMA based nonlinear energy sink with negative stiffness and friction", *Soil Dyn. Earthq. Eng.*, **140**, p. 106466. http://doi.org/10.1016/j.soildyn.2020.106466

De Domenico, D. and Gandelli, E. (2021), "Advanced modeling of SMA flag-shaped hysteresis for nonlinear time-history analysis in SAP2000", *J. Struct. Eng.*, **147**(11), p. 06021004. http://doi.org/10.1061/(ASCE)ST.1943-541X.0003176

De Domenico, D., Gandelli, E. and Quaglini, V. (2020), "Adaptive isolation system combining low-friction sliding pendulum bearings and SMA-based gap dampers", *Eng. Struct.*, **212**, p. 110536. http://doi.org/10.1016/j.engstruct.2020.110536

Den Hartog, J.P. (1947), *Mechanical Vibrations*, McGraw-Hill, New York, USA.

Dieng, L., Helbert, G., Chirani, S.A., Lecompte, T. and Pilvin, P. (2013), "Use of shape memory alloys damper device to mitigate vibration amplitudes of bridge cables", *Eng. Struct.*, **56**, 1547-1556. http://doi.org/https://doi.org/10.1016/j.engstruct.2013.07.018

Ghasemi, M.R., Shabakhty, N. and Enferadi, M.H. (2019), "Vibration control of offshore jacket platforms through shape memory alloy pounding tuned mass damper (SMA-PTMD)", *Ocean Eng.*, **191**, p. 106348. http://doi.org/10.1016/j.oceaneng.2019.106348

Gur, S., Mishra, S.K., Bhowmick, S. and Chakraborty, S. (2014), "Compliant liquid column damper modified by shape memory alloy device for seismic vibration control", *Smart Mater. Struct.*, **23**(10), p. 105009. http://doi.org/10.1088/0964-1726/23/10/105009

Huang, H. and Chang, W. (2018), "Application of pre-stressed SMA-based tuned mass damper to a timber floor system", *Eng. Struct.*, **167**, 143-150. http://doi.org/10.1016/j.engstruct.2018.04.011

Huang, H., Chang, W.-S. and Mosalam, K.M. (2017), "Feasibility of shape memory alloy in a tuneable mass damper to reduce excessive in-service vibration: Feasibility of shape memory alloy in a tuneable mass damper", *Struct. Control. Health Monit.*, **24**(2), p. e1858. http://doi.org/10.1002/stc.1858

Huang, H., Mosalam, K.M. and Chang, W. (2020), "Adaptive tuned mass damper with shape memory alloy for seismic application", *Eng. Struct.*, **223**, 111171. http://doi.org/10.1016/j.engstruct.2020.111171

Koh, J. (2018), "Design of shape memory alloy coil spring actuator for improving performance in cyclic actuation", *Materials*, **11**(11), 2324. http://doi.org/10.3390/ma11112324

Kumbhar, S.B., Chavan, S.P. and Gawade, S.S. (2018), "Adaptive tuned vibration absorber based on magnetorheological elastomer-shape memory alloy composite", *Mech. Syst. Signal Proc.*, **100**, 208-223. http://doi.org/10.1016/j.ymssp.2017.07.027

Liu, A., Liu, C., Fu, J., Pi, Y., Huang, Y. and Zhang, J. (2017), "A method of reinforcement and vibration reduction of girder bridges using shape memory alloy cables", *Int. J. Struct. Stab. Dyn.*, **17**(07), 1750076. http://doi.org/10.1142/S0219455417500766

Lu, Z., Liu, X.Q., Ma, N.Y. and Zhou, M.Y. (2022), "Multi-objective optimization and seismic performance verification of multiple tuned impact dampers for nonlinear benchmark building", *Structures*, **41**, 1672-1686. http://doi.org/10.1016/j.istruc.2022.05.101

Lv, H. and Huang, B. (2023a), "Parametric study of a new tuned mass damper with pre-strained SMA helical springs for vibration reduction", *Smart Struct. Syst., Int. J.*, **31**(1), 89-100. http://doi.org/10.12989/sss.2023.31.1.089

Lv, H. and Huang, B. (2023b), "Vibration reduction performance of a new tuned mass damper with pre-strained superelastic SMA helical springs", *Int. J. Struct. Stab. Dyn.*, **24**(5), p. 250047. http://doi.org/10.1142/S0219455424500470

Ma, R., Bi, K. and Hao, H. (2021), "Inerter-based structural vibration control: A state-of-the-art review", *Eng. Struct.*, **243**, p. 112655. http://doi.org/https://doi.org/10.1016/j.engstruct.2021.112655

Mani, Y. and Senthilkumar, M. (2015), "Shape memory alloy-based adaptive-passive dynamic vibration absorber for vibration control in piping applications", *J. Sound Vib.*, **21**(9), 1838-1847. http://doi.org/10.1177/1077546313492183

Manzoni, S., Argentino, A., Lucà, F., Berardengo, M. and Vanali, M. (2023), "SMA-based adaptive tuned mass dampers: Analysis and comparison", *Mech. Syst. Signal Proc.*, **186**, 109883.

http://doi.org/10.1016/j.ymssp.2022.109883
Mirzai, N.M., Mansouri, I., Tezcan, J., Awoyera, P.O. and Hu, J.W. (2021), "Estimating optimum parameters of a new SMA damper under different earthquake ground motions", *Structures*, **33**, 2700-2712. http://doi.org/https://doi.org/10.1016/j.istruc.2021.06.019
Mishra, S.K., Gur, S. and Chakraborty, S. (2013), "An improved tuned mass damper (SMA-TMD) assisted by a shape memory alloy spring", *Smart Mater. Struct.*, **22**(9), p. 095016. http://doi.org/10.1088/0964-1726/22/9/095016
Mohsenian, V., Filizadeh, R., Hajirasouliha, I. and Garcia, R. (2021), "Seismic performance assessment of eccentrically braced steel frames with energy-absorbing links under sequential earthquakes", *J. Build. Eng.*, **33**, p. 101576. http://doi.org/https://doi.org/10.1016/j.jobe.2020.101576
Moraes, Y.J.O., Rodrigues, M.C., Silva, A.A., Grassi, E.N.D. and Araujo, C.J. (2023), "Vibration control systems in a building prototype: Application of SMA coil springs in diagonal bracing and TMD", *Eng. Struct.*, **275**, p. 115319. http://doi.org/10.1016/j.engstruct.2022.115319
Pasala, D.T.R. and Nagarajaiah, S. (2014), "Adaptive-length pendulum smart tuned mass damper using shape-memory-alloy wire for tuning period in real time", *Smart Struct. Syst., Int. J.*, **13**(2), 203-217. http://doi.org/10.12989/sss.2014.13.2.203
Pinkaew, T., Lukkunaprasit, P. and Chatupote, P. (2003), "Seismic effectiveness of tuned mass dampers for damage reduction of structures", *Eng. Struct.*, **25**(1), 39-46. http://doi.org/https://doi.org/10.1016/S0141-0296(02)00115-3
Qiu, C.X., Zhang, Y.C., Qi, J. and Li, H. (2018), "Seismic behavior of properly designed CBFs equipped with NiTi SMA braces", *Smart Struct. Syst., Int. J.*, **21**(4), 479-491. http://doi.org/10.12989/sss.2018.21.4.479
Rong, K.J. and Lu, Z. (2021), "Performance of a gas-spring tuned mass damper under seismic excitation", *Struct. Eng. Mech., Int. J.*, **80**(2), 157-168. http://doi.org/10.12989/sem.2021.80.2.157
Rong, K. and Lu, Z. (2022), "A novel nonlinear gas-spring TMD for the seismic vibration control of a MDOF structure", *Struct. Eng. Mech.*, **83**(1), 31-43. http://doi.org/10.12989/sem.2022.83.1.031
Rong, K., Lu, Z., Zhang, J., Zhou, M. and Huang, W. (2023), "Nonlinear gas-spring DVA for seismic response control: Experiment and numerical simulation", *Eng. Struct.*, **283**, p. 115940. http://doi.org/https://doi.org/10.1016/j.engstruct.2023.115940
Rustighi, E., Brennan, M.J. and Mace, B.R. (2005a), "Real-time control of a shape memory alloy adaptive tuned vibration absorber", *Smart Mater. Struct.*, **14**(6), p. 1184. http://doi.org/10.1088/0964-1726/14/6/011
Rustighi, E., Brennan, M.J. and Mace, B.R. (2005b), "A shape memory alloy adaptive tuned vibration absorber: design and implementation", *Smart Mater. Struct.*, **14**(1), 19-28. http://doi.org/10.1088/0964-1726/14/1/002
Santos, F.A.D. and Nunes, J. (2017), "Toward an adaptive vibration absorber using shape-memory alloys, for civil engineering applications", *J. Intell. Mater. Syst. Struct.*, **29**(5), 729-740. http://doi.org/10.1177/1045389X17721031
Sgobba, S. and Marano, G.C. (2010), "Optimum design of linear tuned mass dampers for structures with nonlinear behaviour", *Mech. Syst. Signal Proc.*, **24**(6), 1739-1755. http://doi.org/https://doi.org/10.1016/j.ymssp.2010.01.009
Song, G., Ma, N. and Li, H.N. (2006), "Applications of shape memory alloys in civil structures", *Eng. Struct.*, **28**(9), 1266-1274. http://doi.org/10.1016/j.engstruct.2005.12.010
Tian, L., Liu, J., Qiu, C. and Rong, K. (2019), "Temperature effect on seismic behavior of transmission tower-line system equipped with SMA-TMD", *Smart Struct. Syst., Int. J.*, **24**(1), 1-14. http://doi.org/10.12989/sss.2019.24.1.001
Tian, L., Zhou, M., Qiu, C., Pan, H. and Rong, K. (2020), "Seismic response control of transmission tower-line system using SMA-based TMD", *Struct. Eng. Mech., Int. J.*, **74**(1), 129-143. http://doi.org/10.12989/sem.2020.74.1.129
Tiwari, N.D., Gogoi, A., Hazra, B. and Wang, Q. (2021), "A shape memory alloy-tuned mass damper inerter system for passive control of linked-SDOF structural systems under seismic excitation", *J. Sound Vib.*, **494**, p. 115893. http://doi.org/10.1016/j.jsv.2020.115893
Torra, V., Carreras, G., Casciati, S. and Terriault, P. (2014), "On the NiTi wires in dampers for stayed cables", *Smart Struct. Syst., Int. J.*, **13**(3), 353-374. http://doi.org/10.12989/sss.2014.13.3.353
Wang, L. and Melnik, R.V.N. (2012), "Nonlinear dynamics of shape memory alloy oscillators in tuning structural vibration frequencies", *Mechatronics*, **22**(8), 1085-1096. http://doi.org/10.1016/j.mechatronics.2012.09.004
Williams, K., Chiu, G. and Bernhard, R. (2002), "Adaptive-passive absorbers using shape-memory alloys", *J. Sound Vib.*, **249**(5), 835-848. http://doi.org/10.1006/jsvi.2000.3496
Zuo, H. and Zhu, S. (2022), "Development of novel track nonlinear energy sinks for seismic performance improvement of offshore wind turbine towers", *Mech. Syst. Signal Proc.*, **172**, 108975. http://doi.org/10.1016/j.ymssp.2022.108975
Zuo, H., Bi, K., Hao, H. and Ma, R. (2021), "Influences of ground motion parameters and structural damping on the optimum design of inerter-based tuned mass dampers", *Eng. Struct.*, **227**, p. 111422. http://doi.org/10.1016/j.engstruct.2020.111422
Zuo, H., Bi, K., Hao, H. and Li, C. (2022), "Numerical study of using shape memory alloy-based tuned mass dampers to control seismic responses of wind turbine tower", *Eng. Struct.*, **250**, p. 113452. http://doi.org/10.1016/j.engstruct.2021.113452.